Exchange bias in a columnar nanocrystalline $Ni_{80}Fe_{20}$/CoO thin film

J. van Lierop and B. W. Southern
Department of Physics and Astronomy, University of Manitoba, Winnipeg, MB, R3T 2N2, Canada

K.-W. Lin and Z.-Y. Guo
Department of Materials Engineering, National Chung Hsing University, Taichung 402, Taiwan

C. L. Harland
Australian Synchrotron Research Program, c/o ANSTO, PMB 1, Menai, NSW, 2234, Australia

R. A. Rosenberg and J. W. Freeland
Advanced Photon Source, Argonne National Laboratory, 9700 South Cass Avenue, Argonne, Illinois 60439, USA
(Received 1 August 2007; revised manuscript received 29 October 2007; published 28 December 2007)

The effects of interfacial coupling at the boundary of ferromagnetic and antiferromagnetic components in a nanoscale columnar-structured thin film of $Ni_{80}Fe_{20}$/CoO have been examined. Field-cooling the film results in very different temperature dependences of the enhanced coercivity and exchange-bias shift of the hysteresis loop. The exchange-bias temperature dependence is well described by thermal fluctuations of the interfacial spins while the coercivity temperature dependence indicates that single-domain-like columns are being coherently rotated by the thermal fluctuations of the interface spins. Furthermore, only a portion of the spins in the antiferromagnetic layer seem to be associated with the spin coupling that results in exchange bias. X-ray magnetic resonant scattering measurements show clearly the presence of canted Co interfacial moments that provide a local field which enables exchange bias at a significantly higher temperature than the onset of an enhanced coercivity.

DOI: 10.1103/PhysRevB.76.224432 PACS number(s): 75.30.Et, 75.70.Cn, 75.75.+a

I. INTRODUCTION

At the interface between ferromagnetic and antiferromagnetic materials, exchange coupling is thought to lead to a unidirectional anisotropy. This unidirectional anisotropy is presumed to arise from order in the antiferromagnet being established in the presence of a field that causes the antiferromagnetic interfacial moments to tilt away from their preferred direction towards an orientation that is similar to that of the ferromagnetic spin moments. These canted moments couple to the ferromagnetic moments and are believed to be weakly affected by subsequent changes in the external field at lower temperatures. During the measurement of a magnetic hysteresis loop, the resulting torque on the ferromagnetic moments creates the observed (exchange bias) loop shift away from the zero-field axis. An additional observed result of the exchange coupling is an enhanced coercivity compared to the pure ferromagnetic film. The current experimental and theoretical understanding of exchange bias is described in recent review articles.[1–3]

Although the phenomenology of exchange coupling is understood, the fundamental mechanism remains unclear. A difficulty in understanding the basic physics is the characterization and understanding of the interface structure and morphology, properties that are strongly dependent upon deposition technique and conditions. Furthermore, a key issue central to the physics of exchange bias is the temperature dependence of the interfacial coupling that affects both the measured coercivity and exchange-bias loop shift.

Models of exchange bias typically describe the loop shift as the result of coupling between the first layers of the ferromagnetic and antiferromagnetic materials,[4]

$$H_{ex} = \frac{2J_{ex}\vec{S}_F \cdot \vec{S}_{AF}}{a_F^2 M_F t_F}, \tag{1}$$

where J_{ex} represents the interfacial exchange coupling that is believed to be related to the ferromagnetic and antiferromagnetic exchange stiffness constants. $\vec{S}_F$ and $\vec{S}_{AF}$ are the interfacial spins in the ferromagnet (FM) and antiferromagnet (AF) layers, t_F the ferromagnet layer thickness, a_F the lattice constant of the ferromagnet, and M_F the magnetization density of the ferromagnetic layer. While application of Eq. (1) (with bulk material properties values) results in values of J_{ex} that are typically an order of magnitude too large to explain measured loop shift (H_{ex}) values,[2,3] more interfacially detailed models remedy this issue. The incomplete ferromagnetic domain-wall model that describes the AF interfacial spins as being canted with respect to the ferromagnetic interfacial spins and the external measuring field[5] is such a model. The theoretical treatment of a temperature dependence of antiferromagnetic grains in an exchange-coupled system[6] is another successful treatment that predicts similar $H_{ex}(T)$ behavior as the previous model.

The enhanced coercivity that is another experimental hallmark of exchange coupling has been the topic of separate theoretical investigations.[2,3] A description of the enhanced coercivity as arising from inhomogeneous reversal and irreversible transitions in the antiferromagnetic grains of a polycrystalline thin-film system[7] provides a qualitative agreement with experimental work, while temperature-dependent domain-wall behavior in the antiferromagnetic component of a film has also been successfully applied.[8,9]

As a departure from the typical textured, multidomain thin-film geometry[2,3] and to improve the comprehension of the physics behind exchange bias, we have synthesized a nanoscale columnar-structured thin film that provides a different interface geometry. The film consists of a polycrystalline ~20-nm $Ni_{80}Fe_{20}$ layer on top of a ~15-nm CoO polycrystalline layer, both layers having ~10-nm-diameter columns that penetrate the whole film thickness. Field-cooling the film from 350 K results in a strong temperature-dependent enhanced coercivity $H_c(T)$ and exchange bias shift $H_{ex}(T)$ of the hysteresis loop. $H_c(T)$ exhibits a very different temperature dependence than $H_{ex}(T)$. While $H_{ex}(T)$ is well described by thermal fluctuations of the antiferromagnetic exchange-coupled interfacial moments[5,10] described in a mean-field approximation, the coercivity behaves much more like that of a ferromagnetic single-domain particle in the low-temperature limit. This temperature behavior indicates that the ferromagnetic single-domain-like columns are being coherently rotated by the thermal fluctuations of the interface spins. At the lowest temperatures, there is a marked increase in $H_c(T)$ and $H_{ex}(T)$ that may be the result of intercolumnar interactions dominating the energetics that results in different magnetic reversal mechanisms for increasing and decreasing applied fields.

II. EXPERIMENTAL METHODS

A dual ion-beam deposition technique was used to make the thin film.[11] The system consists of a Kaufman deposition source and an End-Hall-assisted source. The Kaufman source is used to focus an argon ion beam onto a target surface (either $Ni_{80}Fe_{20}$ or Co) while the End-Hall source is used to clean or *in situ* bombard the substrate during deposition with an oxygen-argon mixture. An approximately 15-nm-thick CoO film was deposited on top of a Si(100) substrate with a 20-nm $Ni_{80}Fe_{20}$ capping film. No external field was used during deposition. A MAC Science (MXP18) analytical x-ray system with Cu $K\alpha$ radiation was used to provide x-ray diffraction data, while a JEOL (JEM-2010) transmission electron microscope (TEM) operating at 200 kV was used for microstructural analysis. Magnetometry and susceptometry studies were performed in a Quantum Design Physical Property Measurement System, where the film was field cooled (with the film in the 50-kOe field plane) from 350 K down through the antiferromagnetic (Néel) transition temperature.

Polarized x-ray techniques were used at beamline 4-ID-C of the Advanced Photon Source[12] to characterize the element-resolved magnetism of the film. The experimental configuration allowed simultaneous measurement of the grazing incidence x-ray absorption and scattering while switching between left-circular polarization (I^+) and right-circular-polarization (I^-) in magnetic fields up to 70 kOe. Information about the electronic environment is provided by the sum ($I^+ + I^-$) of these signals, and magnetic information is contained in the difference ($I^+ - I^-$), which in absorption and scattering are referred to, respectively, as x-ray magnetic circular dichroism[13] (XMCD) and x-ray resonant magnetic scattering[14,15] (XRMS). Element-specific hysteresis was measured using field-dependent resonant scattering since the 20-nm $Ni_{80}Fe_{20}$ top film layer absorbed a significant component of the incident photons. Ni and Co elemental hysteresis measurements were achieved by measuring the change in scattering intensity with magnetic field at a fixed scattering angle of 9° (Refs. 14 and 15). The $Ni_{80}Fe_{20}$/CoO film was field cooled in 10 kOe from room temperature to 10 K, and ±1 kOe hysteresis loops were collected with warming to determine the Ni and Co contributions to the total H_c and H_{ex}. XRMS signals at 50 K for Ni, Fe, and Co at their respective L_3 edges were collected to ascertain their respective contributions to H_c and H_{ex}.

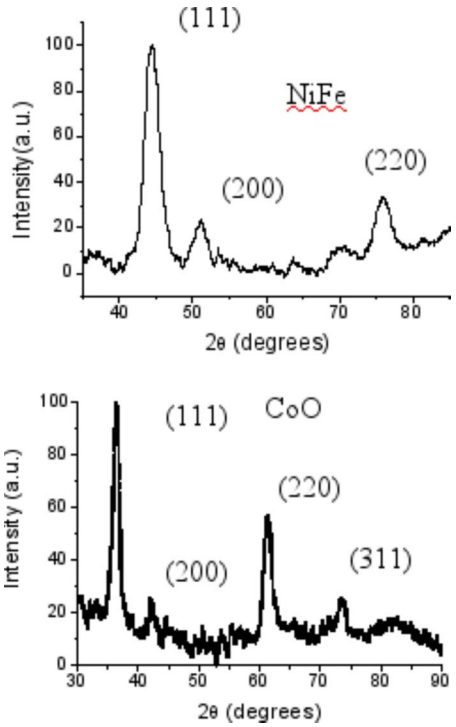

FIG. 1. (Color online) Measured grazing-angle x-ray diffraction patterns of $Ni_{80}Fe_{20}$ (top) and CoO (bottom) films. The CoO film was deposited with a 8% O_2/Ar gas ratio (Ref. 11)

III. RESULTS AND DISCUSSION

Pure $Ni_{80}Fe_{20}$ and CoO thin films made with the same deposition conditions as the $Ni_{80}Fe_{20}$/CoO bilayer were examined with grazing-angle x-ray diffraction to determine the structure and composition of the top and bottom layers of the thin film (Fig. 1). The ferromagnetic $Ni_{80}Fe_{20}$ layer grew with a (111)-preferred orientation and had a cubic lattice constant of 3.53±0.02 Å while the antiferromagnetic CoO film consisted of a rocksalt structure with a lattice constant of 4.27±0.05 Å. The lattice constant of the CoO film component is slightly larger than the bulk value and is likely due to oxygen incorporation during film deposition.

Plane-view TEM images and diffraction patterns were collected to ascertain the average crystallite size and confirm the structure of the film components. Results are shown in Fig. 2. The microstructure consisted of fine equiaxed grains of $Ni_{80}Fe_{20}$ and CoO that appear to extend throughout the

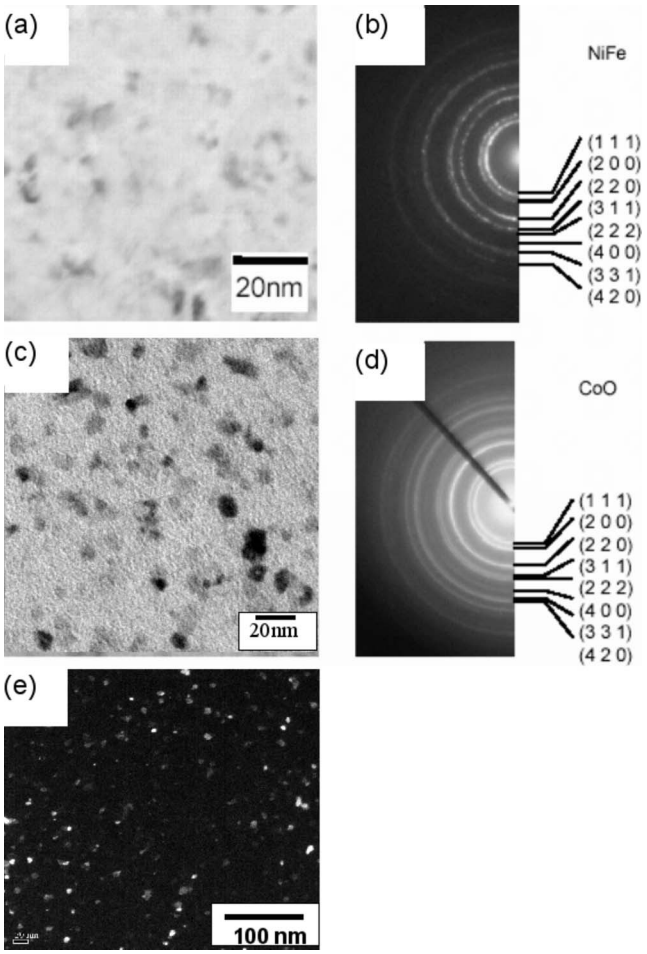

FIG. 2. Plane-view transmission electron microscope images of the $Ni_{80}Fe_{20}$ (a) and CoO (b) films with respective diffraction patterns in (b) and (d). (e) is a lower-resolution dark-field image of the CoO film showing the dispersion of nanocolumns.

film thickness (Fig. 3). The electron diffraction patterns are in excellent agreement with the assignments described by the x-ray diffraction patterns. Grain sizes averaged 10 nm (as determined from bright- and dark-field images) and are significantly smaller then the film thickness (Fig. 3). The cross-sectional TEM micrograph in Fig. 3 shows that the $Ni_{80}Fe_{20}$ layer has a thickness of ~20 nm and the CoO layer is ~15 nm thick. These results also show that each polycrystalline layer has a columnar structure that is perpendicular to the film surface with no obvious interdiffusion between the $Ni_{80}Fe_{20}$ and CoO interface. Furthermore, the CoO lattice spacing can be clearly seen (Fig. 3) and has been determined to be $d_{111}=2.49\pm0.02$ Å.

Even if finite-size effects modify Curie temperature of the 20-nm $Ni_{80}Fe_{20}$ layer from its bulk value of T_C 800 K,[16] T_C will be well above the maximum measuring temperature of these experiments ($T_{max}=350$ K). However, the nanoscale nature of the 15-nm CoO film may also affect the Néel temperature (T_N) of this component. Knowledge of T_N is important for understanding the nature of the exchange coupling and setting the range of temperatures through which to field-cool the film. To determine T_N, zero-field-cooled ac susceptibility (χ_{ac}) measurements were done using a 10-Oe drive

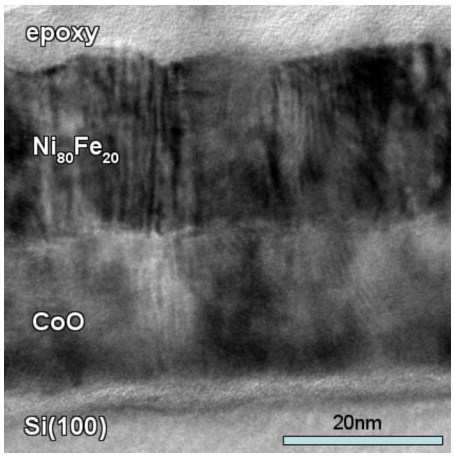

FIG. 3. (Color online) Cross-sectional TEM micrograph of the $Ni_{80}Fe_{20}$/CoO bilayer grown on a Si(100) surface.

field at the measuring frequencies shown in Fig. 4. At low to intermediate temperatures the in-phase (χ'_{ac}) and out-of-phase (χ''_{ac}) components are essentially temperature and frequency independent, indicating that the AF CoO layer spin moments are static and ordered. Between ~200 and 275 K, with warming, there is a gradual increase in $\chi'_{ac}(T)$ while $\chi''_{ac}(T)$ remains constant. We attribute this behavior to AF canted spins at the film interface undergoing a shift from a static, frozen configuration towards a fluctuating arrangement (see below). Finally, there is a marked increase in $\chi'_{ac}(T)$ between ~275 and 300 K, after which $\chi'_{ac}(T)$ is essentially constant upon further warming. In addition, there is a measured peak in $\chi''_{ac}(T)$ (inset, Fig. 4) that is centered around 290 K. The frequency-independent nature of $\chi_{ac}(T)$ as well as the rapid increase of the in-phase and peak in the out-of-phase (dissipative) components around 290 K is strong evidence that the temperature scan has passed through the transition (Néel) temperature of the AF CoO film component. Furthermore, the measured $T_N \sim 290$ K is in excellent agreement with the T_N of bulk CoO.[16]

A suggestion of the relative orientation of the FM and AF moment spins during the temperature evolution of the exchange coupling is provided by the $\chi_{ac}(T)$ data in Fig. 4. Assuming that the FM and AF moment orientations with respect to a field are determined by the bulk magnetocrystalline anisotropies[2,16] ($K_F=-3\times10^3$ erg/cm^3 and $K_{AF}=5\times10^5$ erg/cm^3), at low temperatures, it should be energetically favorable for the $Ni_{80}Fe_{20}$ FM spins to align with the small (10 Oe) measuring field, while the CoO spins should be aligned antiferromagnetically perpendicular to the applied field. This picture should hold except for the first few layers of interfacial AF spins that will be torqued into the plane of the FM moment spins. With increasing temperature as the AF Néel temperature is approached, AF spins will cant over into the direction of the FM layer, adding to the measured magnetization, as seen in Fig. 4.

Additional evidence of the AF interfacial coupling affecting the magnetism of the FM layer is provided by the measured saturation magnetization (M_s) of the film. For a similarly constructed pure $Ni_{80}Fe_{20}$ film, we measured an

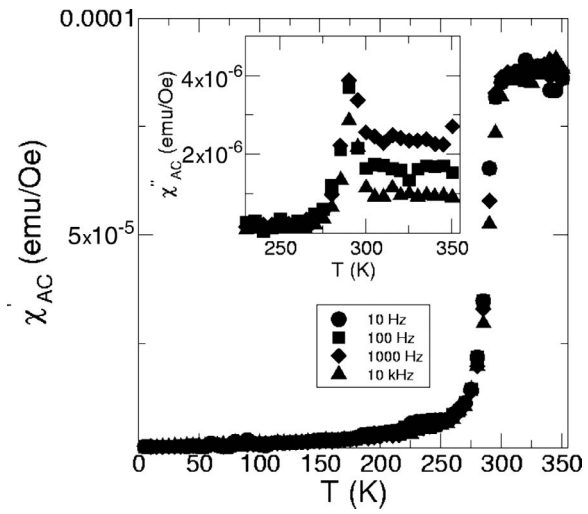

FIG. 4. In-phase component of the temperature-dependent ac susceptibility (χ'_{ac}) of the $Ni_{80}Fe_{20}$ thin film. The inset shows the out-of-phase component of χ''_{ac} around the antiferromagnetic CoO Néel transition.

essentially temperature-independent[17] $M_s \sim 630$ emu/cm^3. However, for the $Ni_{80}Fe_{20}$/CoO film, we found a temperature-independent[17] $M_s = 300 \pm 10$ emu/cm^3, which indicates that the $Ni_{80}Fe_{20}$ film component has a $M_s \sim 530$ emu/cm^3 (since this layer makes up 60% of the film volume). This ~20% reduction of the FM M_s is another hint that there is a canted spin component in the AF layer with an average magnetization that is counter to the FM film element.

Magnetic scattering measurements provide the most convincing evidence of a canted spin component at the $Ni_{80}Fe_{20}$/CoO interface. Figure 5(a) shows the XRMS signal at 50 K of the Fe, Ni, and Co spins. The Fe and Ni are FM components and a nonzero XRMS signal is expected; however, the Co atoms are present in the AF CoO, which should provide no change in scattering intensity with magnetic field.[15] There is a clear Co XRMS signal that can only be the result of canted Co moments. The interfacial Co magnetization contribution results in a shift of the Co hysteresis loop along the field (H) and magnetization (intensity) axis, shown in Fig. 5(b). The difference in $+H$ and $-H$ Co saturation magnetizations indicates that the Co canted moment orientation is opposite to that of the $Ni_{80}Fe_{20}$, which is the origin of the measured 20% reduction of M_s described above.

The inset in Fig. 6 shows a typical M versus H loop after field-cooling the film in 50 kOe with a clear exchange-bias loop shift H_{ex}. The interface energy $\Delta E = H_{ex} t_F M_F = 0.14 \pm 0.02$ erg/cm^2 at 10 K is a measure of the FM/AF exchange coupling strength and is in good agreement with other polycrystalline CoO-based bilayers.[3] Using a ferromagnetic domain wall model,[5] the high-temperature to midtemperature H_{ex} temperature evolution is well described (solid line in Fig. 6). In this model, the first AF interface layer is frozen into a canted spin configuration and couples to the FM layer where FM single-domain width columns of nanocrystallites are rotated. $H_{ex}(T)$ is simply a measure of this temperature-dependent coupling and is predicted to follow[10]

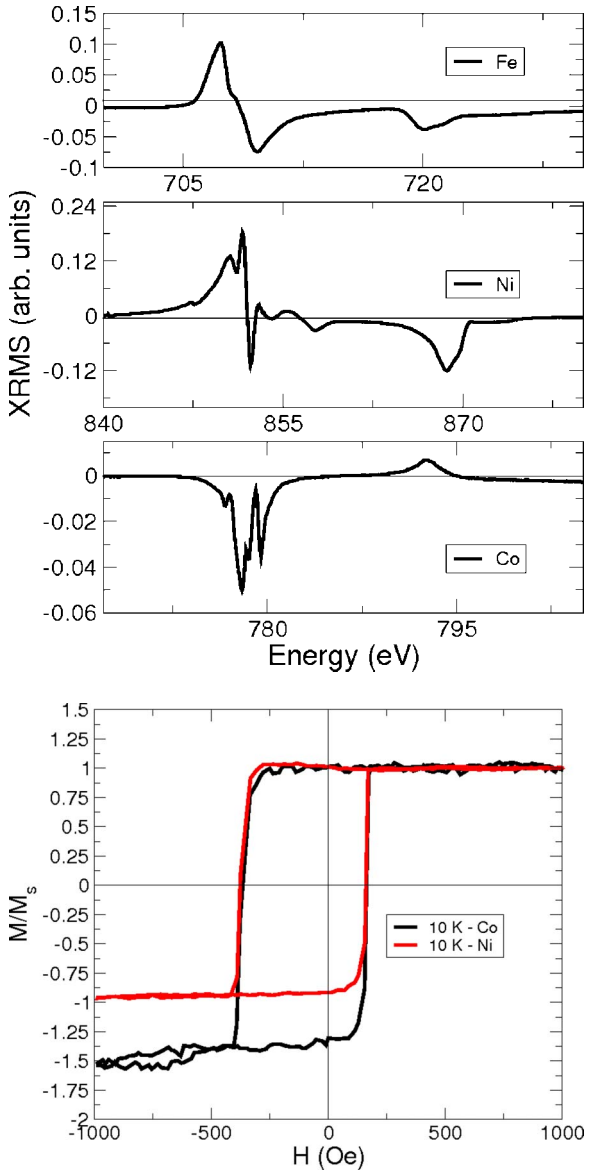

FIG. 5. (Color online) (a) XRMS at the Fe, Ni, and Co L_3 edges at 50 K. Nonzero XRMS provides a clear indication of the canted Co interfacial moment. (b) Ni and Co elemental hysteresis loops at 10 K after field cooling.

$$H_{ex}(T) = \frac{2 J_F B_S(x) \kappa a_F}{g_F \mu_B t_F}, \tag{2}$$

with J_F the FM exchange stiffness constant of the $Ni_{80}Fe_{20}$, a_F the FM crystal lattice constant, $g_F = 2.2$ the FM g factor, μ_B the Bohr magneton, and t_F the FM layer thickness. The spins at the FM/AF interface are expected to exhibit a mean-field temperature dependence given by the Brillouin function $B_S(x)$ with $x = -z J_{AF} \langle S \rangle_T / (k_B T)$ where z is the number of nearest AF neighbors in the bulk and J_{AF} is the AF exchange stiffness constant. The interface coupling energy is described by an effective coupling constant[10]

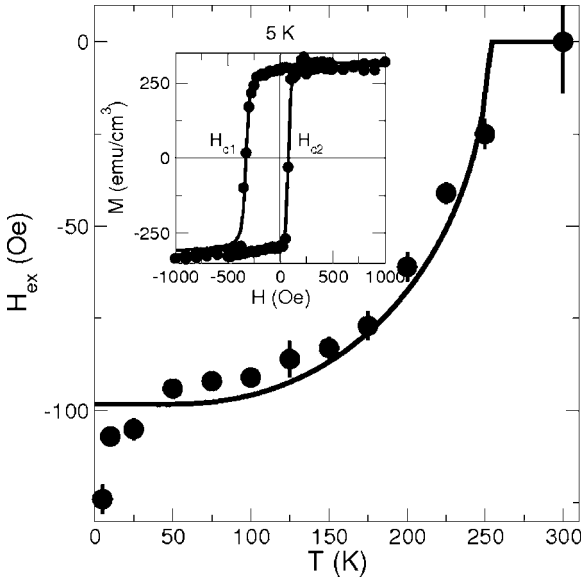

FIG. 6. Exchange-bias field $H_{ex}=(H_{c1}+H_{c2})/2$ as a function of temperature after field-cooling the $Ni_{80}Fe_{20}/CoO$ film in a 50-kOe field. The solid line is to a fit described in the text. The inset shows a typical hysteresis loop at 5 K after being field cooled.

$$\kappa = \frac{|J_{ex}|}{J_F}\left[\frac{2|J_{ex}| - g_{AF}\mu_B H_{cf}}{10|J_{AF}| + 2K_{AF}}\right], \tag{3}$$

where J_{ex} is the exchange coupling constant, J_{AF} is the AF exchange stiffness constant, $g_{AF}=2$ is the AF g factor, H_{cf} is the cooling field applied to set the exchange bias, and K_{AF} is the bulk AF magnetocrystalline anisotropy.

Essentially this formalism describes $H_{ex}(T)$ arising when the ratio of exchange energies in Eq. (2) is appropriate so that an exchange-bias loop shift occurs, while the curvature is basically set by the magnitude of J_{AF} and the maximum H_{ex} determined by J_{ex}. Assuming that $S=1$ and using values from the literature for bulk $Ni_{80}Fe_{20}$ and CoO for J_F, $g_{F/AF}$, z,[10,16] and J_{AF},[18] and the measured value of a_F, with $H_{cf}=50$ kOe, a nonlinear least-squares fit of $H_{ex}(T)$ (solid line in Fig. 6) yields a $J_{AF}=8.2\pm0.1$ meV and $J_{ex}=0.002\pm0.001$ meV. These values are in good agreement with other exchange-biased thin-film systems.[10,19] The relatively large value of the fitted J_{AF} is consistent with exchange-biased thin-film systems with large K_{AF} [e.g., $Ni_{81}Fe_{19}/Ir_{22}Mn_{78}$ (Ref. 19)] as is the exchange coupling constant. The temperature dependence of H_{ex} is a result of strong interfacial coupling at the FM/AF interface, with interfacial spins well described by a mean-field-like temperature dependence (in a sense the interfacial spins are ordering with cooling into a canted configuration). The low-temperature (below 50 K) $H_{ex}(T)$ is decreasing, and not accounted for in the above theoretical description of the exchange coupling, and suggests that the magnetization reversal mechanism has changed for increasing and decreasing fields, and may be due to interchain coupling of AF spins in the AF nanocolumns beginning to appear at low temperatures.

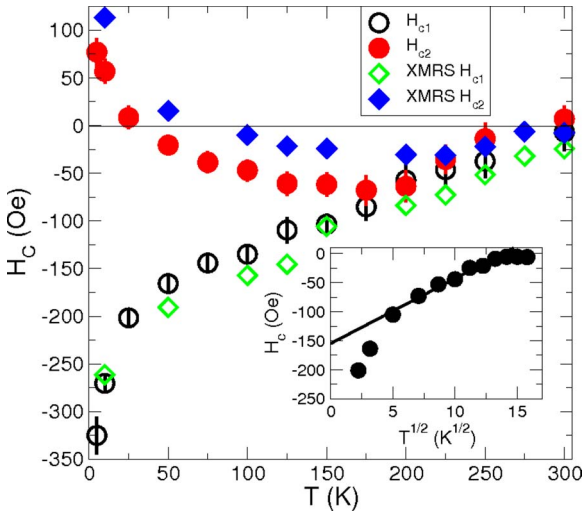

FIG. 7. (Color online) Left (H_{c1}) and right (H_{c2}) coercivities measured by magnetometer (○) and XRMS (◇) after the $Ni_{80}Fe_{20}/CoO$ film was field cooled, with H_{c1} and H_{c2} values determined from field-cooled hysteresis loop measurements. The inset shows $H_c(T)=(H_{c1}-H_{c2})/2$ from the magnetometry studies as a function of $\sqrt{T}$. The solid line is a guide to the eye.

The pure $Ni_{80}Fe_{20}$ thin film had a coercivity (H_c) of ~6 Oe.[11] Exchange-coupling results in an enhanced coercivity H_c (with respect to the pure ferromagnetic component[2,3]), and this enhanced H_c is observed in this $Ni_{80}Fe_{20}/CoO$ thin-film sample (Fig. 7). While the interfacial spin temperature evolution between 300 K and 50 K is well described by a Brillouin function [Eq. (2) for $H_{ex}(T)$], analysis of the left (H_{c1}) and right (H_{c2}) coercive fields in Fig. 7 reveals a very unusual nanomagnetism due to the interplay between the nanocolumnar $Ni_{80}Fe_{20}$ and CoO. At temperatures between ~200K and T_N we see that while there is a loop shift, $H_c(T)=[H_{c1}(T)-H_{c2}(T)]/2$ remains essentially constant with temperature. This atypical exchange-bias behavior is in the same range of temperatures marked by the dramatic temperature increase of $\chi'_{ac}(T)$ to T_N shown in Fig. 4 that we attributed to the establishment of interfacial ordering and concomitant exchange coupling between the $Ni_{80}Fe_{20}$ and CoO moments for individual nanocolumns. This magnetic interplay between $H_c(T)$ and $H_{ex}(T)$ is in contrast to previously observed exchange-bias behavior in polycrystalline $Ni_{80}Fe_{20}/CoO$ thin films where both $H_c(T)$ and $H_{ex}(T)$ display a strong temperature dependence over the same range of temperatures[20] in a manner well described by current models[6,7,19,21] and typical of most exchange-bias film systems.[2,3] The experimental results on this $Ni_{80}Fe_{20}$ (20 nm)/CoO (15 nm) film seem to indicate that exchange coupling is providing a "local field" at the interface[22,23] that shifts the hysteresis loop. Only when strong enough exchange coupling is present (below ~250 K) is domain wall rotation perturbed that enables different $H_{c1}(T)$ and $H_{c2}(T)$.

There are two customary descriptions of the physics of the enhanced coercivity in exchange-bias bilayers. One description rests on the domain-wall behavior in the AF layer[8,9] with an assumed mean-field dependence of the antiferromagnetic magnetocrystalline anisotropy to characterize $H_c(T)$.

The other account is based on the idea that an enhanced H_c arises from inhomogeneous reversal and irreversible transitions in the AF grains,[7] with $H_c(T)$ behavior that is also essentially mean-field-like. While both these descriptions adequately characterize the usual[2,3] $H_c(T)$ behavior, the measured $H_c(T)$ in our $Ni_{80}Fe_{20}$/CoO columnar nanocrystalline film cannot be described by the above models. Current descriptions of $H_c(T)$ predict a rapid temperature evolution near T_N that is followed by an essentially constant $H_c(T)$. Our experimental results on this $Ni_{80}Fe_{20}$/CoO thin film present the opposite to this modeled behavior, with no temperature dependence in $H_c(T)$ near T_N and a rapid low-temperature $H_c(T)$

Experimental studies of polycrystalline NiFe (30 nm)/CoO, where the CoO layer varied from 10 nm to 300 nm,[24,25] show a similar mean-field $H_{ex}(T)$ dependence as our nanocolumnar $Ni_{80}Fe_{20}$ (20 nm)/CoO (15 nm) film; however, no information on $H_c(T)$ was provided. A description based on uncompensated AF interface spins was offered to explain $H_{ex}(T)$,[25] which is consistent with our description using Eq. (2). For a polycrystalline 20-nm-thick NiFe film deposited onto a bulk single crystal of CoO, a very different, linear temperature dependence of H_c and H_{ex} was observed.[20] Recent work on the thickness dependence of $H_c(T)$ in Fe/MnF_2 thin films has shown that there is a significant change in $H_c(T)$ with FM thickness[26] from 1.8 nm to 16 nm. In the Fe/$MnFe_2$ films, $H_c(T)$ is essentially linear with temperature for thin FM layers, and with increasing FM thickness $H_c(T)$ is better described by a Brillouin function. The reports on $H_c(T)$ in these systems do not agree with $H_c(T)$ shown in the inset to Fig. 7. In addition, it is worth noting that in the nanocolumnar $Ni_{80}Fe_{20}$/CoO thin film, a clear exchange-bias loop shift is observed at temperatures significantly above that where an enhanced coercivity (both negative and positive field) temperature dependence develops.

To further investigate this different $H_c(T)$ behavior, we have performed M versus H measurements of the Ni moments in the $Ni_{80}Fe_{20}$ layer and the Co moments in the CoO layer using XRMS. Since XRMS is sensitive to net FM alignment of the Ni and Co, we are able to directly measure the coercivity from the canted magnetization of the CoO interface moments. Figure 7 shows the results of the elemental Ni and Co H_c's renormalized with respect to the amount of each element in the film and their respective magnetizations, as shown in Fig. 5(a).[27] The slight difference in H_c's between the magnetometry and XRMS measurements can be attributed to the different field-cooling procedures (50 kOe from 350 K to 5 K for the magnetometry studies and 10 kOe from 300 K to 10 K for the XRMS studies) and magnetic field environments at the sample due to the different solenoids with their respective magnetic field profiles. In addition, the Fe contribution to the total H_c, while presumably not large, is missing from the XRMS results. The local magnetism of the Ni moments in the $Ni_{80}Fe_{20}$ and the Co moments in the CoO film components probed by XRMS exhibits the same $H_{c1}(T)$ and $H_{c2}(T)$ behavior. This agreement between independent measuring techniques singularly identifies the measured nanomagnetism as intrinsic to the nanocolumnar $Ni_{80}Fe_{20}$/CoO thin film. Furthermore, the agreement between the different measuring techniques and field-cooling protocols tells us that the unusual exchange-bias loop shift with constant $H_c=(H_{c1}-H_{c2})/2$ at temperatures between 200 K and 300 K is entirely due to the interfacial exchange coupling. Insight into the different physics of the nanomagnetism between $H_{ex}(T)$ and $H_c(T)$ in this nanocolumnar $Ni_{80}Fe_{20}$ thin-film system is provided by the $H_c(T)$ versus $\sqrt{T}$ dependence above ~25 K, show by the solid line in the inset plot in Fig. 7. Typically, this type of temperature dependence of the coercivity is associated with coherent domain-wall motion that is related to a thermally activated process.[16] A further indication of this activation process is provided by the weak frequency dependence of $\chi'_{ac}(T)$ at temperatures below T_N [the scale required to show the compete range of $\chi'_{ac}(T)$ in Fig. 4 obscures this frequency dependence]. This thermally activated mechanism driving $H_c(T)$ is quite different in origin from the Brillouin temperature dependence of the interfacial moment ordering demarked by Eq. (2) for $H_{ex}(T)$. At temperatures below 25 K, $H_{ex}(T)$ and $H_c(T)$ are likely dominated by interchain moment coupling between the $Ni_{80}Fe_{20}$ and CoO nanocolumns that provides a enhanced energy barrier to domain-wall reversal.

In conclusion, to better understand the physics of exchange bias, we have examined the temperature dependence of the coercivity H_c and exchange-bias loop shift H_{ex} in a columnar nanocrystalline $Ni_{80}Fe_{20}$/CoO thin film. The temperature dependences of H_c and H_{ex} are quite different; however, the basic magnetic spin behaviors of the FM layer, at the FM/AF interface and in the AF layer, are all based on thermal fluctuations of the spins. The rotation of domains responsible for $H_c(T)$ is well described by an activated energy picture, while exchange coupling seems to result in a layer of canted AF spins at the interface that are characterized by thermal fluctuations described in a mean-field approximation, implying that a sort of order is being set in the interfacial spins with cooling. The observed mix of temperature behavior of $H_c(T)$ and $H_{ex}(T)$ indicates that the interface spins responsible for H_{ex} are dragging the single-domain FM columns in a coherent fashion that is responsible for the observed activated energy temperature dependence. This is in contrast to the traditional theoretical view that AF single-domain clusters are responsible for $H_c(T)$ and $H_{ex}(T)$.[2,3,7,21]

ACKNOWLEDGMENTS

This work was supported by grants from the Natural Sciences and Engineering Research Council of Canada and in part by the National Science Council of Taiwan under Grant No. NSC-93-2216-E-005-019. Use of the Advanced Photon Source was supported by the U.S. Department of Energy, Office of Science, Office of Basic Energy Sciences, under Contract No. DE-AC02-06CH11357.

[1] J. Nogués, J. Sort, V. Skumryev, S. Suriñach, J. S. Muñoz, and M. D. Baró, Phys. Rep. **422**, 65 (2005).
[2] A. E. Berkowitz and K. Takano, J. Magn. Magn. Mater. **200**, 552 (1999).
[3] J. Nogués and I. K. Schuller, J. Magn. Magn. Mater. **192**, 203 (1999).
[4] A. P. Malozemoff, Phys. Rev. B **37**, 7673 (1988).
[5] J. Mejía-López, R. Ramírez, and M. Kiwi, J. Magn. Magn. Mater. **241**, 2002 (2002).
[6] M. D. Stiles and R. D. McMichael, Phys. Rev. B **60**, 12950 (1999).
[7] M. D. Stiles and R. D. McMichael, Phys. Rev. B **63**, 064405 (2001).
[8] V. I. Nikitenko, V. S. Gornakov, L. M. Dedukh, Y. P. Kabanov, A. F. Khapikov, A. J. Shapiro, R. D. Shull, A. Chaiken, and R. P. Michel, Phys. Rev. B **57**, R8111 (1998).
[9] J. Wang, W. N. Wang, X. Chen, H. W. Zhao, J. G. Zhao, and W. S. Zhan, Appl. Phys. Lett. **77**, 2731 (2000).
[10] J. Mejía-López, D. Altbir, and I. K. Schuller, Appl. Phys. Lett. **83**, 332 (2003).
[11] K. W-Lin, F. T-Lin, and Y. M-Tzeng, Jpn. J. Appl. Phys., Part 1 **44**, 04R12047 (2005).
[12] J. W. Freeland, J. C. Lang, G. Srajer, R. W. Winarski, D. Shu, and D. M. Mills, Rev. Sci. Instrum. **73**, 1408 (2002).
[13] C. T. Chen, Y. U. Idzerda, H.-J. Lin, N. V. Smith, G. Meigs, E. Chaban, G. H. Ho, E. Pellegrin, and F. Sette, Phys. Rev. Lett. **75**, 152 (1995).
[14] C. Kao, J. B. Hastings, E. D. Johnson, D. P. Siddons, G. C. Smith, and G. A. Prinz, Phys. Rev. Lett. **65**, 373 (1990).
[15] J. B. Kortright and S.-K. Kim, Phys. Rev. B **62**, 12216 (2000).
[16] R. C. O'Handley, *Modern Magnetic Materials, Principles and Applications* (Wiley, New York, 2000).
[17] The film volume for the magnetic measurements was estimated with an areal measurement and corrorborated with a Si substrate volume calculation using the measured high-field diamagnetic susceptibility signal from the 0.15-mm-thick substrate.
[18] O. Nakanishi and T. Yamada, J. Phys. Soc. Jpn. **36**, 1315 (1974).
[19] H. Xi, R. M. White, Z. Gau, and S. Mao, J. Appl. Phys. **92**, 4828 (2002).
[20] T. J. Moran, J. M. Gallego, and I. K. Schuller, J. Appl. Phys. **78**, 1887 (1995).
[21] E. Fulcomer and S. H. Charap, J. Appl. Phys. **43**, 4190 (1972).
[22] J. van Lierop, K. W. Lin, J. Y. Guo, H. Ouyang, and B. W. Southern, Phys. Rev. B **75**, 134409 (2007).
[23] H. Ouyang, K. W. Lin, C. C. Liu, S. C. Lo, Y. M. Tzeng, J. Y. Guo, and J. van Lierop, Phys. Rev. Lett. **98**, 097204 (2007).
[24] K. Takano, R. H. Kodama, A. E. Berkowitz, W. Cao, and G. Thomas, Phys. Rev. Lett. **79**, 1130 (1997).
[25] K. Takana, R. H. Kodama, A. E. Berkowitz, W. Cao, and G. Thomas, J. Appl. Phys. **83**, 6888 (1998).
[26] C. Leighton, M. R. Fitzsimmons, A. Hoffmann, J. Dura, C. F. Majkrzak, M. S. Lund, and I. K. Schuller, Phys. Rev. B **65**, 064403 (2002).
[27] J. van Lierop, B. W. Southern, K. W. Lin, J. Y. Guo, H. Ouyang, R. A. Rosenberg, J. W. Freeland, and C. L. Harland (unpublished).